Applied Physics Letters

Magnon and spin transition contribution in heat capacity of ferromagnetic Cr-doped MnTe: Experimental evidence for a paramagnetic spin-caloritronic effect

Cite as: Appl. Phys. Lett. **117**, 043903 (2020); https://doi.org/10.1063/5.0011887
Submitted: 25 April 2020 . Accepted: 15 July 2020 . Published Online: 28 July 2020

Md Mobarak Hossain Polash, Morteza Rasoulianboroujeni, and Daryoosh Vashaee

Applied Physics Letters ARTICLE scitation.org/journal/apl

Magnon and spin transition contribution in heat capacity of ferromagnetic Cr-doped MnTe: Experimental evidence for a paramagnetic spin-caloritronic effect

Cite as: Appl. Phys. Lett. **117**, 043903 (2020); doi: 10.1063/5.0011887
Submitted: 25 April 2020 · Accepted: 15 July 2020 ·
Published Online: 28 July 2020

Md Mobarak Hossain Polash,[1,2] Morteza Rasoulianboroujeni,[3] and Daryoosh Vashaee[1,2,a)]

AFFILIATIONS

[1]Department of Materials Science and Engineering, NC State University, Raleigh, North Carolina 27606, USA
[2]Department of Electrical and Computer Engineering, NC State University, Raleigh, North Carolina 27606, USA
[3]School of Dentistry, Marquette University, Milwaukee, Wisconsin 53233, USA

[a)]Author to whom correspondence should be addressed: dvashae@ncsu.edu

ABSTRACT

We present experimental evidence for the simultaneous existence of the magnons and spin-state transition contributions to the heat capacity in ferromagnetic (FM) Cr-doped MnTe ($T_c \sim 280$ K), where the magnon heat capacity is attributed to the observed magnon-bipolar carrier-drag thermopower. The pristine antiferromagnetic (AFM) MnTe shows only a magnon-induced peak in the heat capacity near the Néel temperature, $T_N \sim 307$ K. However, Cr-doped MnTe shows a magnon-contributed heat capacity peak at ~293 K with an additional peak in the deep paramagnetic domain near 780 K. Temperature-dependent magnetic susceptibility reveals that Cr-doping initially creates low-spin (LS) state Mn^{2+} ions into MnTe near and below T_N due to a higher crystal field induced by Cr ions. Above 400 K, LS Mn^{2+} ions start converting into high-spin (HS) Mn^{2+} ions. The LS-to-HS transition of Mn^{2+} leads to an excess entropy and hence excess heat capacity contribution in the system. Temperature-dependent X-ray diffraction (XRD) and magnetic field-dependent susceptibility (M-H) confirmed no presence of any structural changes and magnetic polaron, respectively. Both XRD and M-H ensure that the peak of the heat capacity in the paramagnetic domain is originated solely by the spin-state transition. The heat capacity vs temperature was calculated to explain the contribution of each component, including the ones due to the phonons, magnons, spin-transition, Schottky anomaly, and lattice dilation. With the recent advances in spin-caloritronics extending the spin-based effects from magnetic to paramagnetic materials, the data from the heat capacity can play a crucial role to probe the presence of different phenomena, such as paramagnon-carrier-drag and spin-entropy thermopowers.

The interest in magnetic semiconductors for thermoelectric research is overgrowing due to the demonstrations of promising spin-caloritronic effects, such as spin-Seebeck,[1] magnon-drag,[2,3] magnon-bipolar drag,[4] paramagnon-drag,[5] and spin-entropy[6] effects. Over the past two decades, the progress in thermoelectric research has been primarily dominated by finding methods for reducing the thermal conductivity of the materials, such as increasing the phonon scattering via nano inclusions[7–12] and nanostructuring.[13,14] Some other techniques have been developed to enhance the power factor with increasing the thermopower, such as carrier filtering,[15–18] carrier pocket engineering,[19–21] complex structures,[22–24] creation of resonant energy levels close to the band edges,[25] and low dimensional structures.[26,27] The spin-based phenomena are of particular interest as they offer alternate routes to enhance the thermopower, which can be combined with nanostructuring methods to reduce the thermal conductivity simultaneously. The paramagnon-drag and spin-entropy, in particular, extend the spin-caloritronic effects to the paramagnetic phase, which opens a much larger domain for thermoelectric material search and innovation along with the magnetic semiconductors.[4,5,28] In this regard, the progress in magnetic and paramagnetic thermoelectrics relies on complementary spin-related characterizations, in addition to the standard thermoelectric property measurements, to better understand and benefit from the spin-based effects.

As thermopower is the amount of entropy carried by the carriers, heat capacity is one of the effective methods to probe the presence of different entropy carriers, such as lattice vibrations (phonons), charge

carriers, spin, and orbital degree of freedoms.[29] Typically, heat capacity can have contributions from lattice (C_v), electronic (C_e), magnon (C_m), Schottky anomaly (C_{sc}), dilation (C_d), and spin transition (C_{st}), which are directly related to those degrees of freedoms.[30] A distinct sharp peak appears in the heat capacity due to the latent heat associated with the first-order transitions, such as lattice structure or some magnetic phase changes in the materials. In contrast, the second-order transitions, such as spin-state transitions and Schottky effects, show a broad peak in C_p, which is related to the changes in the free energy per molecule.[31] From the contributors of the heat capacity, distinct information on energetics,[32] thermal, electrical, and lattice properties[33] can be obtained.

In this work, we demonstrated the existence of the specific heat contributions from both quantized spin-wave or magnons at the magnetic transition temperature and spin-state transition in the paramagnetic domain in Cr-doped MnTe (Fig. 1). Interestingly, Cr-doped MnTe showed magnon-bipolar carrier-drag, and spin-transition influenced thermopower at the corresponding temperatures,[4,28] which can be related to the excess entropy of the system created by the spin degree of freedoms. Among spin-based contributions, magnonic contribution to the heat capacity has been widely reported;[3,5,31,33] however, the spin transition contribution has been demonstrated only in a few materials.[31,32] In addition, both of these contributions in the same material were rarely reported[31] and never reported in any MnTe-based systems. MnTe is a widely studied material in spintronics and spin-caloritronics research due to its benevolent spin properties.[5,28,34–36] The heat capacity of pristine MnTe is shown in Fig. 1 and is compared to that of Cr-doped MnTe ($Mn_{0.95}Cr_{0.05}Te$). While MnTe shows a single magnon heat capacity contribution from the spin system near the Néel temperature, $Mn_{0.95}Cr_{0.05}Te$ shows an additional peak in the paramagnetic phase. In the following, we will discuss the nature of this peak.

MnTe and 5% Cr-doped MnTe were made from pure (99.99%) elemental powders. Elemental powders were milled for 8 h in a tungsten carbide cup with a proper ratio under the Ar environment to ensure a uniform mixture. The milled powders were sealed in quartz tubes under vacuum and annealed at 850 °C for 24 h in a rocking furnace to achieve uniform doping distribution. The annealed materials were milled again with the same recipe. Finally, the powders were consolidated in graphite dies with spark-plasma-sintering at 950 °C with a heating rate of ∼60 °C/min and a soaking time of 20 min under a 50 MPa pressure and an Ar environment. The spark plasma sintering (SPS) was performed inside the glovebox and under an inert atmosphere with <0.01 ppm O_2 and H_2O levels to prevent oxidation of the material. The consolidated ingots were >97% dense. They were characterized by a Rigaku Miniflex X-ray diffractometer at room temperature and with a PANalytical Empyrean X-ray diffractometer at higher temperatures. A Quantum Design DynaCool 12T Physical Property Measurement System (PPMS) was used to measure the low-temperature C_p and magnetic susceptibility, and a Netzsch differential scanning calorimetry (DSC 404 F1) was used for the high-temperature C_p measurement.

The first peak in the heat capacity of both MnTe and $Mn_{0.95}Cr_{0.05}Te$ appeared at ∼306 K and ∼293 K, respectively. Both peaks are from the magnon contribution. MnTe is an antiferromagnetic (AFM) semiconductor with the NiAs structure and a Néel temperature of $T_N \sim 307$ K, while $Mn_{0.95}Cr_{0.05}Te$ is an isostructural ferromagnetic (FM) semiconductor with a Curie temperature of $T_c \sim 280$ K, as shown in Fig. 2. Cr-doping into MnTe substitutes Mn^{2+} with Cr^{3+} and acts as an electron donor into MnTe.[4,37] It also creates an FM phase by making AFM–FM clustering due to the competition between FM and AFM exchange interactions.[4,38] The alternate potential reasons for the FM phase in Cr-doped MnTe are a canted-spin structure and the spin-polarized hole-mediated ferromagnetic interaction.[4,38] However, the magnon contributed C_p near the Néel temperature of MnTe and the FM trends observed in the inverse magnetic susceptibility (Fig. 2) support the former reason for the magnetic nature of $Mn_{0.95}Cr_{0.05}Te$.[4]

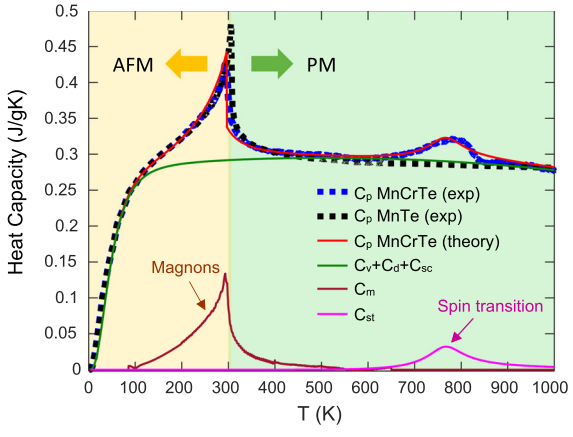

FIG. 1. Heat capacity (C_p) of $Mn_{0.95}Cr_{0.05}Te$ (blue) and MnTe (black) as a function of temperature. C_p plot shows a distinct sharp peak associated with magnon in the magnetic domain (yellow background) and a broad peak associated with the spin-state transition in the paramagnetic domain (green background). Lattice, dilation, and Schottky contributions (green) along with magnonic (brown) and spin transition (magenta) contributions, and the total calculated C_p (red) are estimated from mathematical models.[31]

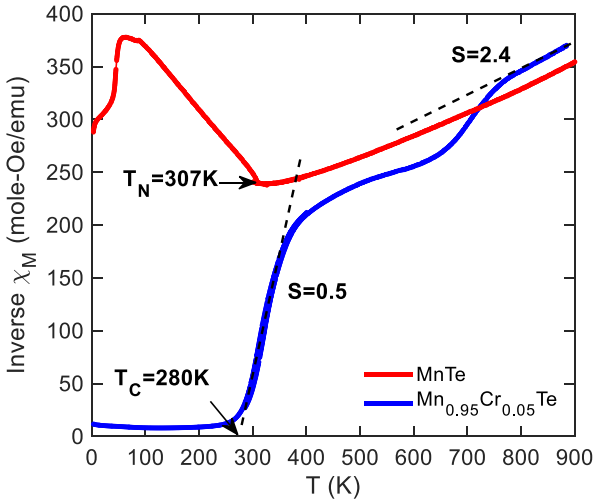

FIG. 2. Inverse magnetic susceptibility of AFM MnTe (red) and FM $Mn_{0.95}Cr_{0.05}Te$ (blue) under the magnetic field of 1000 Oe. The corresponding Néel and Curie temperatures and the spin numbers calculated from the Curie–Weiss law are shown.

Spin numbers for both MnTe and $Mn_{0.95}Cr_{0.05}Te$ are calculated by applying the Curie–Weiss law on the inverse susceptibility in the paramagnetic domain. Mn^{2+} in MnTe has a spin number of around 2.4 in the paramagnetic domain, which indicates its high spin (HS) state, while the combination of Mn^{2+} and Cr^{3+} in $Mn_{0.95}Cr_{0.05}Te$ shows a distinct spin transition from low spin (LS) of 0.5 to HS of 2.4. Here, all Cr^{3+} ions are always in the HS ($S = 1.5$) state due to the $3d^3$ electronic configuration. The lower concentration of Cr^{3+} signifies that Mn^{2+} controls the spin numbers and the corresponding spin-state transition characteristics of $Mn_{0.95}Cr_{0.05}Te$. It is likely that Cr^{3+} ions increase the crystal field in MnTe, which induces the LS state of Mn^{2+} up to about 400 K. Figure 3 illustrates the AFM superexchange interactions between Mn^{2+}(HS)–Mn^{2+}(HS) in MnTe and Mn^{2+}(LS)–Mn^{2+}(LS) in $Mn_{0.95}Cr_{0.05}Te$ via Te^{2-} p orbitals. The presence of the weak Mn–Mn and Mn–Cr AFM bonding, along with the strong Cr–Cr FM bonding, can reduce the C_p peak in $Mn_{0.95}Cr_{0.05}Te$ compared to that in MnTe.[4]

At high temperatures, LS Mn^{2+} is transitioned to HS Mn^{2+} by overcoming the crystal field due to both the electron–electron repulsion and the available thermal energy. At comparable crystal field and Hund's exchange energy, both LS and HS ions can coexist, which is often observed in d^n transition-metal compounds ($4 \leq n \leq 7$).[39] With the increase in temperature, three events can occur: a continuous LS to HS transition, a first-order LS–HS transition, or a thermal depletion of the HS ground state.[39] However, the broad peak in C_p indicates a continuous LS to HS transition. Other possible reasons for the excess entropy contribution can be the second-order displacive crystal-structure change[31] and magnetic entropy from short-range ferromagnetic correlation in the paramagnetic domain, which can cause a phonon instability and provide some contribution to C_p.[31,40] To confirm the underlying reason for the broad C_p peak in $Mn_{0.95}Cr_{0.05}Te$, we carried out both magnetic moment vs magnetic field (M-H) and the X-ray diffraction (XRD) at different temperatures. The M-H plot can reveal the presence of short-range ferromagnetic correlation, also known as bound magnetic polaron (BMP).[40] However, the M-H

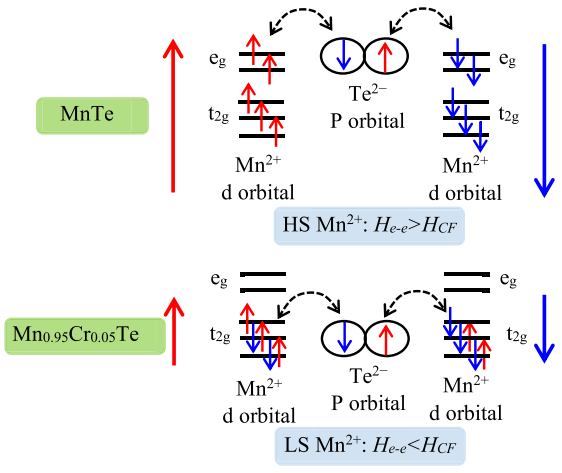

FIG. 3. Mn–Mn AFM superexchange interactions in MnTe and $Mn_{0.95}Cr_{0.05}Te$. Cr-induced high crystal field energy (H_{CF}) higher than the electron–electron repulsion energy (H_{e-e}) shifts Mn^{2+} from the HS into the LS state leading to a weak Mn–Mn AFM superexchange interaction.

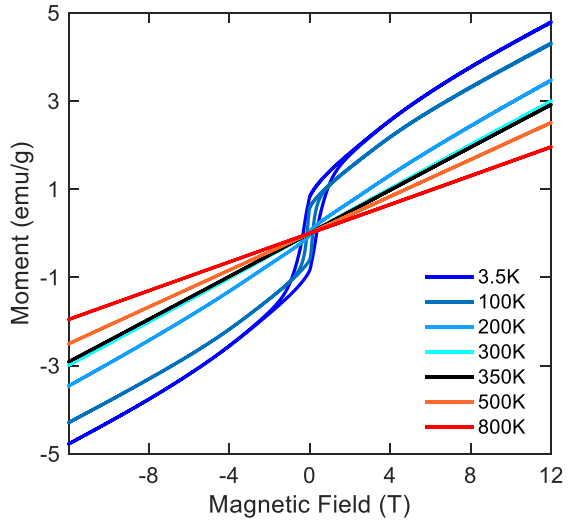

FIG. 4. Magnetic moment of $Mn_{0.95}Cr_{0.05}Te$ vs magnetic field at different temperatures.

trends at different temperatures from different magnetic phase domains in Fig. 4 show that $Mn_{0.95}Cr_{0.05}Te$ is completely paramagnetic above 300 K without any trace of BMPs.

To detect any crystal structure change at the temperature range of interest, a heated XRD was performed at 400, 600, and 850 K. The obtained data are illustrated in Fig. 5. The XRD at different temperatures has the same features, which indicates that there are no crystal changes. The lack of evidence for BMPs and crystal change suggests that the broad peak of C_p is due to the LS to HS transition of Mn^{2+}, which is happening at this range of temperature. Based on the observations from XRD, we can also eliminate the Jahn–Teller (JT) effect as a contributing factor in C_p.

In Cr-doped MnTe below ~400 K, we have LS Mn^{2+} ions with $3d^5$ and HS Cr^{3+} ions with $3d^3$ configuration. Above ~400 K, we have HS Mn^{2+} ions with $3d^5$ and HS Cr^{3+} ions with $3d^3$ configuration. They are both in octahedral coordinates. The HS d^5 and HS d^3 ions do

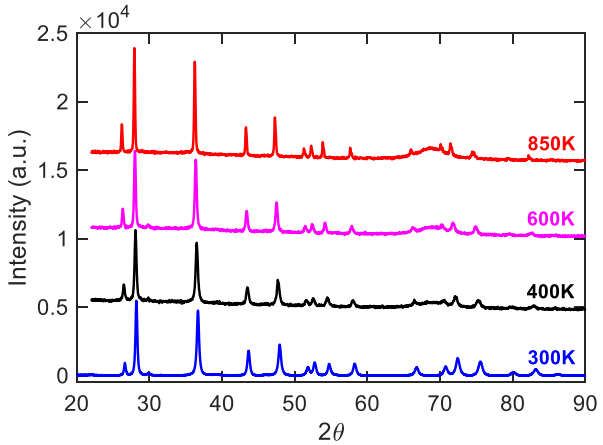

FIG. 5. XRD patterns of $Mn_{0.95}Cr_{0.05}Te$ at different temperatures.

not experience a JT effect due to a lack of degeneracy, while LS d^5 ions in the octahedral coordinate can have a weak JT effect. In Cr-doped MnTe, we can also have Mn^{3+} ($3d^4$) and Cr^{2+} ($3d^4$) ions, which can have a JT effect, but their concentration is small (<5%). Therefore, with the insignificant amount of ions with the JT effect (<5%) and majority JT inactive ions (>95%), Cr-doped MnTe is expected to have an insignificant JT effect at high temperatures (>400 K), where we observe the spin-transition mediated C_p peak. However, at low temperatures (<400 K), a weak JT effect in Cr-doped MnTe can exist. Furthermore, JT distortion is expected to add new peaks in the temperature-dependent XRD.[41,42] However, the temperature-dependent XRD pattern of Cr-doped MnTe showed no modification in the number or position of the diffraction peaks. This matter agrees with our expectation that Cr-doped MnTe must have no significant JT effect at high temperatures.

Due to the similarities of $Mn_{0.95}Cr_{0.05}Te$ heat capacity trends and those of MnTe, except a smaller magnon-induced peak at ~293 K and the broad peak at a higher temperature, lattice, Schottky, and dilation contributions to C_p can be considered to be similar for both materials, and those contributions have already been reported for MnTe.[33] Electronic heat capacity contribution is calculated using the relation for a non-degenerate narrow bandgap semiconductor $C_e = \gamma T = 3.5nk_BT$,[43] where γ is the electronic heat capacity constant, n is the carrier concentration, and k_B is the Boltzmann constant. For $Mn_{0.95}Cr_{0.05}Te$, the γ is calculated as $\sim 4 \times 10^{-8}$ J/gK^2, assuming an approximate carrier concentration of 5×10^{15} cm^{-3}.[4] Hence, C_e is found as 3.2×10^{-5} J/gK at 800 K, which is <0.01% of C_p. The similar non-spin heat capacity contribution in $Mn_{0.95}Cr_{0.05}Te$ as MnTe and its small electronic contribution to C_p support that the differences are mainly due to the magnon and spin-state transition contributions. By eliminating the contribution of non-spin-based contributions from C_p, the maximum magnon heat capacity (C_m) for MnTe is found to be approximately 0.22 J/gK. In comparison, the maximum C_m for $Mn_{0.95}Cr_{0.05}Te$ is estimated to be ~0.16 J/gK. The exchange interaction energies are expected to be less in $Mn_{0.95}Cr_{0.05}Te$ than those in MnTe due to the LS state of Mn^{2+} in $Mn_{0.95}Cr_{0.05}Te$. Therefore, the characteristic temperature, θ_M, related to the magnon ensembles in $Mn_{0.95}Cr_{0.05}Te$ should be less than that in MnTe, because $\theta_M \propto aJSk_M/k_B$.[44] Here, a is the distance between the nearest neighbors, J is the exchange interaction energy, S is the spin number, k_M is the maximum value of the wavevector, which can be obtained from either lattice parameters or the carrier concentration, and k_B is the Boltzmann constant.[44] For AFM semiconductors, the heat capacity contribution from AFM magnon changes as $C_{mag} \propto T^3$, when $T \ll \theta_M$.[44,45]

In Cr-doped MnTe, initially, Mn^{2+} ions are in the LS state; hence, there is a distinct exchange interaction between two adjacent LS Mn^{2+} ions, which is denoted as J_0 (see the supplementary material). Once the LS Mn^{2+} ions transition to the HS state, the exchange interaction energy between two adjacent Mn^{2+} HS ions is different from J_0. The exchange interaction energy for nearest-neighbor HS ions is denoted with J, which is calculated using the following expression:[31,46]

$$J = \Delta - k_BTL - 3Nk_BT\Delta\theta_D{}^2/\theta_D, \quad (1)$$

in which Δ is the energy gap between the LS and HS ground states, N is the number of ions per molecule, $\Delta\theta_D$ is the difference in the Debye temperatures (θ_D) between LS and HS states, Z is the partition function, and T is the temperature.[31] L is a function calculated from the partition function of the HS state (supplementary material). A physical explanation for $\Delta\theta_D$ is discussed in the supplementary material. Based on the Bragg–Williams approximation, the free energy per molecule due to the spin transition is[46]

$$f = (\Delta - k_BTL)n - Jn^2 - k_BT[nlnn - (1-n)ln(1-n)], \quad (2)$$

where n is the HS fraction in the material. The calculated n and f are illustrated in Fig. 6. From the free energy, the heat capacity at a constant volume due to the spin transition can be obtained by using $C_{v,st} = -T\left(\frac{\partial^2 f}{\partial T^2}\right)_v$.[31]

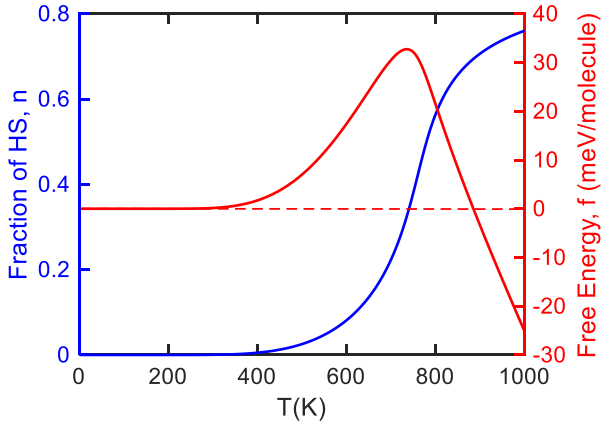

FIG. 6. Fraction of HS ions, n (left axis), and free energy per molecule, f (right axis), in $Mn_{0.95}Cr_{0.05}Te$.

Based on the parameters associated with Mn^{2+} ions,[31] along with some fitting parameters, different magnon, and spin transition-related parameters are calculated, which are shown in Table I. It is worth mentioning that both the peak and shape of the spin-transition contributed heat capacity are very sensitive to the fitting parameters, which does not allow us to vary those parameters more than 10%–15%. This implies that the fitting parameters cannot be too far from the real physical values. The estimated magnon and spin transition heat capacity contributions along with the total heat capacity (considering non-spin heat capacity contributions of MnTe) are illustrated in Fig. 1. A good agreement was found with the experimental data. Details of numerical modeling are discussed in the supplementary material.

TABLE I. The estimated magnon and spin-related parameters for MnTe and $Mn_{0.95}Cr_{0.05}Te$ from experimental data and the numerical model. Experimental values are given in parentheses.

Parameters	MnTe	$Mn_{0.95}Cr_{0.05}Te$
J (meV) (LS Mn^{2+})	…	−16.17
C_{st} (J/gK)	0	0.034 (0.032)
f (meV)	0	33
θ_D (K)	140	140
$\Delta\theta_D$ (K)	…	7
Δ_{LS-HS} (meV)	…	255
ε (meV)	…	15

The trends of the heat capacity data (Fig. 1), magnetic susceptibility (Fig. 2), and the calculated HS faction (Fig. 6) vs temperature agree that the spin transition happens approximately over the temperature range of 400–800 K. Nevertheless, the estimated HS fraction extends to a somewhat higher temperature. According to Fig. 2, a significant spin number change occurs at around 400 K, while Fig. 6 shows only the onset of LS-to-HS at this temperature, which may arise an ambiguity. It should be noted that we have fitted the heat capacity based on the dominant Mn^{2+} LS-to-HS transition; however, the spin transition in Cr-doped MnTe is more complicated and requires a more detailed theoretical study. The magnetic susceptibility trend of Cr-doped MnTe is associated with several spin-transition phenomena. $Mn_{0.95}Cr_{0.05}Te$ consists of two 3d ions, namely, Cr^{3+} and Mn^{2+}, which can transition to Cr^{2+} and Mn^{3+} due to the charge transfer reactions. The XRD data show a small trace of the CrTe impurity phase, which supports the presence of Cr^{2+}.[4,28] The fact that the C_p shows no significant peak associated with the transition near 400 K may also be due to the measurement tolerances. While the heat capacity trend is dominated by the majority of Mn^{2+} ions, the other ions can have nontrivial contributions in the more sensitive magnetic susceptibility measurement. This hypothesis is further evidenced by the presence of several distinct peaks for 3d ions in $Mn_{0.95}Cr_{0.05}Te$ reported by high precision spectroscopy measurements.[4,28]

In summary, two spin-based heat capacity contributions were demonstrated in Cr-doped MnTe, where the former contribution is coming from magnon and the later from the spin transition in the paramagnetic domain. Both spin-based components create excess spin entropy contributing to spin-caloritronic thermopower enhancement in $Mn_{0.95}Cr_{0.05}Te$. The C_p peak due to magnons is almost identical for both MnTe and Cr-doped MnTe. In $Mn_{0.95}Cr_{0.05}Te$, this peak is attributed to the weak AFM exchange interaction. The paramagnetic C_p peak is associated with Mn^{2+} LS, induced by a higher crystal field in $Mn_{0.95}Cr_{0.05}Te$ to Mn^{2+} HS transition at ~780 K. The magnetic susceptibility data agree with the spin transition occurring over the temperature range of 400–800 K. The free energy, heat capacity components, and the fraction of HS Mn^{2+} ions were calculated, which quantified the heat capacity contributions due to magnons and the spin transitions.

See the supplementary material for details of the heat capacity component calculations.

This study is partially based upon the work supported by the Air Force Office of Scientific Research (AFOSR) under contract number FA9550-19-1-0363 and the National Science Foundation (NSF) under Grant Nos. ECCS-1351533, ECCS-1515005, and ECCS-1711253.

DATA AVAILABILITY

The data that support the findings of this study are available within the article and its supplementary material.

REFERENCES

[1]K. Uchida, S. Takahashi, K. Harii, J. Ieda, W. Koshibae, K. Ando, S. Maekawa, and E. Saitoh, Nature **455**, 778–781 (2008).
[2]M. E. Lucassen, C. H. Wong, R. A. Duine, and Y. Tserkovnyak, Appl. Phys. Lett. **99**(26), 262506 (2011).
[3]M. M. H. Polash, F. Mohaddes, M. Rasoulianboroujeni, and D. Vashaee, J. Mater. Chem. C **8**(12), 4049–4057 (2020).
[4]M. M. H. Polash and D. Vashaee, Phys. Rev. B **102**(4), 045202 (2020).
[5]Y. Zheng, T. Lu, M. M. H. Polash, M. Rasoulianboroujeni, N. Liu, M. E. Manley, Y. Deng, P. J. Sun, X. L. Chen, R. P. Hermann, D. Vashaee, J. P. Heremans, and H. Zhao, Sci. Adv. **5**(9), eaat9461 (2019).
[6]Y. Wang, N. S. Rogado, R. J. Cava, and N. P. Ong, Nature **423**, 425–428 (2003).
[7]S. Sumithra, N. J. Takas, D. K. Misra, W. M. Nolting, P. F. P. Poudeu, and K. L. Stokes, Adv. Energy Mater. **1**, 1141–1147 (2011).
[8]Z. Zamanipour and D. Vashaee, J. Appl. Phys. **112**, 093714 (2012).
[9]N. Satyala, J. S. Krasinski, and D. Vashaee, Acta Mater. **74**, 141–150 (2014).
[10]N. Satyala, A. Tahmasbi Rad, Z. Zamanipour, P. Norouzzadeh, J. S. Krasinski, L. Tayebi, and D. Vashaee, J. Appl. Phys. **115**(4), 044304 (2014).
[11]N. Satyala, A. Tahmasbi Rad, Z. Zamanipour, P. Norouzzadeh, J. S. Krasinski, L. Tayebi, and D. Vashaee, J. Appl. Phys. **115**(20), 204308 (2014).
[12]A. Gharleghi, M. M. H. Polash, R. Malekfar, S. A. Yamini, and D. Vashaee, J. Alloys Compd. **845**, 156188 (2020).
[13]P. Norouzzadeh, Z. Zamanipour, J. S. Krasinski, and D. Vashaee, J. Appl. Phys. **112**(12), 124308 (2012).
[14]Z. Zamanipour, X. Shi, A. M. Dehkordi, J. S. Krasinski, and D. Vashaee, Phys. Status Solidi A **209**(10), 2049–2058 (2012).
[15]D. Vashaee and A. Shakouri, Phys. Rev. Lett. **92**(10), 106103 (2004).
[16]M. Dresselhaus, G. Chen, Z. Ren, J. P. Fleurial, P. Gogna, M. Y. Tang, D. Vashaee, H. Lee, X. Wang, G. Joshi, G. Zhu, D. Wang, R. Blair, S. Bux, and R. Kaner, MRS Proc. **1044**(1), 1044-U02-04 (2007).
[17]D. Vashaee and A. Shakouri, Microscale Thermophys. Eng. **8**(2), 91–100 (2004).
[18]D. Vashaee and A. Shakouri, J. Appl. Phys. **101**(5), 053719 (2007).
[19]P. Norouzzadeh and D. Vashaee, Sci. Rep. **6**, 22724 (2016).
[20]P. Norouzzadeh, C. W. Myles, and D. Vashaee, J. Phys.: Condens. Matter **25**(47), 475502 (2013).
[21]P. Norouzzadeh, C. W. Myles, and D. Vashaee, J. Appl. Phys. **114**(16), 163509 (2013).
[22]G. J. Snyder and E. S. Toberer, Nat. Mater. **7**(2), 105–114 (2008).
[23]P. Norouzzadeh, C. W. Myles, and D. Vashaee, Sci. Rep. **4**, 7028 (2014).
[24]L. Tayebi, Z. Zamanipour, and D. Vashaee, Renewable Energy **69**, 166–173 (2014).
[25]J. P. Heremans, V. Jovovic, E. S. Toberer, A. Saramat, K. Kurosaki, A. Charoenpakdee, S. Yamanaka, and G. Snyder, Science **321**, 554 (2008).
[26]D. Vashaee, J. Christofferson, Y. Zhang, A. Shakouri, G. Zeng, C. LaBounty, X. Fan, J. Piprek, J. E. Bowers, and E. Croke, Microscale Thermophys. Eng. **9**(1), 99–118 (2005).
[27]D. Vashaee, Y. Zhang, A. Shakouri, G. Zeng, and Y. J. Chiu, Phys. Rev. B **74**(19), 195315 (2006).
[28]M. M. H. Polash, V. Perelygin, M. Rasoulianboroujeni, Y. Zheng, T. Lu, N. Liu, M. Manley, R. Hermann, A. Smirnov, J. Heremans, H. Zhao, and D. Vashaee, MRS Spring Meeting, Phoenix, Arizona, 22–26 April 2019.
[29]J. He and T. M. Tritt, Science **357**, eaak9997 (2017).
[30]E. S. R. Gopal, *Specific Heats at Low Temperatures* (Plenum Press, New York, 1966).
[31]H. J. Krokoszinski, C. Santandrea, E. Gmelin, and K. Barner, Phys. Status Solidi B **113**, 185 (1982).
[32]S. Stolen, F. Gronvold, H. Brinks, T. Atake, and H. Mori, Phys. Rev. B **55**(21), 14103–14106 (1997).
[33]F. Gronvold, N. J. Kveseth, F. D. S. Marques, and J. Tichy, J. Chem. Thermodyn. **4**, 795–806 (1972).
[34]W. Xie, S. Populoh, K. Gałązka, X. Xiao, L. Sagarna, Y. Liu, M. Trottmann, J. He, and A. Weidenkaff, J. Appl. Phys. **115**, 103707 (2014).
[35]J. Heremans, Y. Zheng, H. Zhao, T. Lu, N. Liu, P. Sun, W. Wang, M. Rasoolianboroujeni, and D. Vashaee, International and European Conference on Thermoelectric, France, 1–5 July 2018.
[36]J. Dong, F.-H. Sun, H. Tang, K. Hayashi, H. Li, P.-P. Shang, Y. Miyazaki, and J.-F. Li, ACS Appl. Mater. Interfaces **11**(31), 28221–28227 (2019).
[37]H. Yadaka, T. Harada, and E. Hirahara, J. Phys. Soc. Jpn. **17**, 875–876 (1962).
[38]Y. B. Li, Y. Q. Zhang, N. K. Sun, Q. Zhang, D. Li, J. Li, and Z. D. Zhang, Phys. Rev. B **72**, 193308 (2005).

[39]R. A. Bari and J. Sivardidre, Phys. Rev. B **5**(11), 4466–4471 (1972).
[40]A. Shahee, K. Singh, R. J. Choudhary, and N. P. Lalla, Phys. Status Solidi B **252**(8), 1832–1838 (2015).
[41]M. Ptak, M. Maczka, A. Gągor, A. Pikul, L. Macalik, and J. Hanuza, J. Solid State Chem. **201**, 270–279 (2013).
[42]A. Segmüller, R. L. Melcher, and H. Kinder, Solid State Commun. **15**, 101–104 (1974).
[43]B. A. Aronzon, G. Galeczki, and G. Nimtz, Philos. Mag. B **67**(6), 847–854 (1993).
[44]C. Kittel, *Quantum Theory of Solids* (John Wiley & Sons, New York, 1963).
[45]J. Van Kranendonk and J. H. Van Vleck, Rev. Mod. Phys. **30**(1), 1–23 (1958).
[46]R. Zimmermann and E. Konig, J. Phys. Chem. Solids **38**(7), 779–788 (1977).